





Zero-field magnetic ground state of EuMg_2Bi_2 Santanu Pakhira ¹, Thomas Heitmann,² S. X. M. Riberolles ¹, B. G. Ueland,¹ R. J. McQueeney,^{1,3}
D. C. Johnston ^{1,3} and David Vaknin ^{1,3}¹Ames Laboratory, Iowa State University, Ames, Iowa 50011, USA²The Missouri Research Reactor and Department of Physics and Astronomy, University of Missouri, Columbia, Missouri 65211, USA³Department of Physics and Astronomy, Iowa State University, Ames, Iowa 50011, USA

(Received 15 September 2020; accepted 18 December 2020; published 8 January 2021)

Layered trigonal EuMg_2Bi_2 is reported to be a topological semimetal that hosts multiple Dirac points that may be gapped or split by the onset of magnetic order. Here, we report zero-field single-crystal neutron-diffraction and bulk magnetic susceptibility measurements versus temperature $\chi(T)$ of EuMg_2Bi_2 that show the intraplane ordering is ferromagnetic (Eu^{2+} , $S = 7/2$) with the moments aligned in the ab plane while adjacent layers are aligned antiferromagnetically (i.e., A-type antiferromagnetism) below the Néel temperature.

DOI: [10.1103/PhysRevB.103.024408](https://doi.org/10.1103/PhysRevB.103.024408)

I. INTRODUCTION

Recent studies of rare-earth-based metallic systems have revealed novel electronic states arising from a complex interplay of magnetism and electron-band topology [1–7]. EuMg_2Bi_2 is one such system that undergoes antiferromagnetic (AFM) ordering below a Néel temperature $T_N \approx 6.7$ K [8–10] and is also reported to host multiple Dirac points located at different energies with respect to the Fermi energy [10]. Various topological states of EuMg_2Bi_2 (such as axion or Weyl states) are dependent on the nature of the magnetic order since time-reversal symmetry breaking and magnetic crystalline symmetry may gap or split the Dirac points.

EuMg_2Bi_2 crystallizes in the trigonal CaAl_2Si_2 -type crystal structure [11] (space group $P\bar{3}m1$, no. 164), where the Eu atoms form a triangular lattice in the ab plane with simple hexagonal stacking along the c axis. Recently, our anisotropic magnetic susceptibility $\chi(T)$ data measured in a magnetic field $H = 1$ kOe demonstrated that both the in-plane and out-of-plane magnetic susceptibilities are almost temperature independent below T_N [8]. Using our recent formulation of molecular-field theory [12,13], it has been proposed that the magnetic structure below T_N is a c -axis helix with a turn angle of $\approx 120^\circ$ between adjacent Eu layers in which the Eu spins are ferromagnetically aligned in the ab plane in each Eu layer [8].

Here, we report neutron-diffraction measurements on single-crystal EuMg_2Bi_2 and determine the zero-field Eu^{2+} spin $S = 7/2$ magnetic structure below T_N to be A-type AFM order with the moments aligned in the ab plane. We also present $\chi(T)$ results in a low magnetic field $H = 100$ Oe that are consistent with the magnetic structure obtained from neutron-diffraction measurements in zero field. The difference between the present AFM structure and that inferred from the previous $\chi(T)$ measurements in $H = 1$ kOe which report a 120° helical structure [8] implies that the magnetic texture (i.e., structure and/or domains) is sensitive to the

strength of the applied magnetic field and requires additional neutron-diffraction measurements under magnetic field for confirmation.

The experimental details and methods are presented in Sec. II. The neutron-diffraction measurements and analyses are discussed in Sec. III and the $\chi(T)$ measurements are discussed in Sec. IV. The results are summarized in Sec. V.

II. EXPERIMENTAL DETAILS AND METHODS

EuMg_2Bi_2 single crystals with hexagonal lattice parameters $a = 4.7724(3)$ and $c = 7.8483(5)$ Å [8] were grown by a self-flux method with starting composition EuMg_4Bi_6 as described previously [9]. The $\chi(T)$ measurements were carried out using a magnetic-properties measurement system (Quantum Design, Inc.) in the temperature range 1.8–300 K. A ≈ 50 -mg crystal was cut into two pieces having masses ≈ 10 and ≈ 40 mg. The 10-mg piece was used for the magnetization measurements and the 40-mg piece was used for neutron-diffraction experiments.

Single-crystal neutron-diffraction experiments were performed in zero applied magnetic field using the TRIAX triple-axis spectrometer at the University of Missouri Research Reactor. An incident neutron beam of energy $E_i = 30.5$ or 14.7 meV was directed at the sample using a pyrolytic graphite (PG) monochromator. Elastic-scattering data were acquired with $E_i = 30.5$ meV in order to reduce the absorption caused by highly absorbing Eu, whereas $E_i = 14.7$ meV was used to improve the resolution in a search for possible peaks associated with an incommensurate magnetic structure. A PG analyzer was used to reduce the background. Neutron wavelength harmonics were removed from the beam using PG filters placed before the monochromator and in between the sample and analyzer. The beam divergence was limited using collimators before the monochromator, between the monochromator and sample, between the sample and ana-

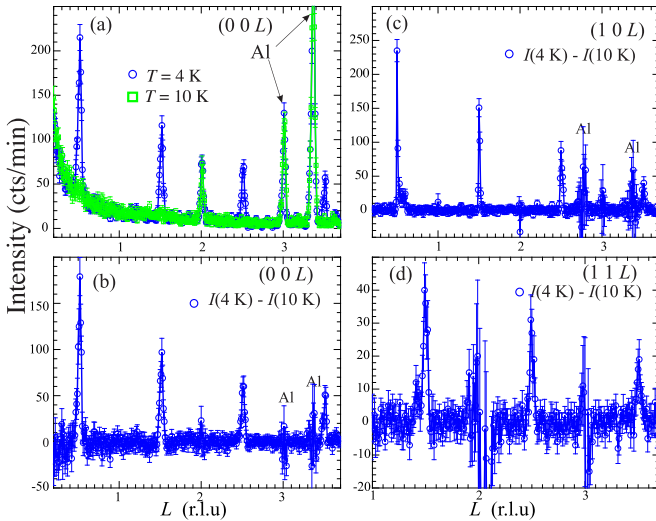


FIG. 1. (a) Diffraction pattern along $(00L)$ of single-crystal EuMg_2Bi_2 at 4 and 10 K as indicated. Aluminum Bragg reflections are from the sample holder. (b) Difference between the $(00L)$ patterns taken at 4 and 10 K. (c) Difference between the $(10L)$ patterns taken at 4 and 10 K. (d) Difference between $(11L)$ patterns taken at $T = 4$ and 10 K. All three difference patterns show clear magnetic peaks at half integer L up to $L = 3.5$, consistent with A-type AFM, i.e., the zero-field ground state is such that the intraplane ordering is ferromagnetic while adjacent layers are aligned antiferromagnetically.

lyzer, and between the analyzer and detector of $60'$, $60'$, $40'$, and $40'$, respectively.

A 40-mg EuMg_2Bi_2 crystal was mounted on the cold tip of an Advanced Research Systems closed-cycle refrigerator with a base temperature of 4 K. The crystal was aligned in the (HHL) and (HOL) scattering planes whereupon a wide range of reciprocal space was accessible for our comparative diffraction study above (10 K) and below $T_N = 6.7$ K (at 4 K). Reciprocal space was searched extensively using a series of H , HH , and L scans as well as mesh scans in order to identify any commensurate or incommensurate wave vectors that might be present.

III. NEUTRON DIFFRACTION

Figure 1(a) shows diffraction scans along $(00L)$ at 4 and 10 K, where reflections at half-integer L values are apparent at $T = 4$ K. For more clarity, Fig. 1(b) shows the difference between these two scans, where within experimental uncertainty there is no evidence for other reflections associated with a modulated structure along the c axis. Similar differences [i.e., $I(4\text{ K}) - I(10\text{ K})$] for scans along $(10L)$ and $(11L)$, shown in Figs. 1(c) and 1(d), respectively, also reveal new peaks at half-integer L values. Qualitatively, these newly emerging Bragg reflections indicate the doubling of the unit cell along the c axis. We also note that the intensities of the new peaks become weaker at larger L values and also as the total momentum transfer Q gets larger [i.e., $Q_{(11L)} > Q_{(10L)} > Q_{(00L)}$], roughly following the falloff expected from the magnetic form factor. These qualitative observations unequivocally establish that these peaks are associated with A-type AFM ordering

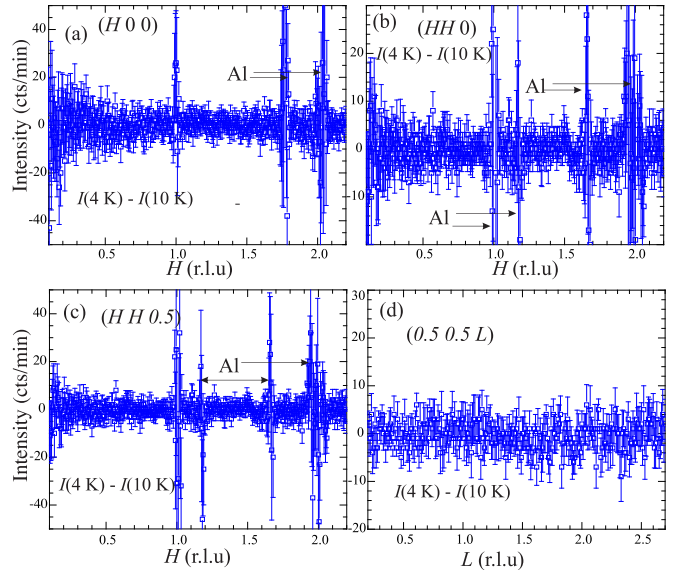


FIG. 2. Difference between the diffraction patterns taken at $T = 4$ and 10 K for (a) $(H00)$, (b) $(HH0)$, (c) $(HH\frac{1}{2})$, and (d) $(\frac{1}{2}\frac{1}{2}L)$ with no indication of nonferromagnetic in-plane magnetic ordering of EuMg_2Bi_2 , which together with Fig. 1 indicate simple A-type antiferromagnetism. The noise is due to thermal changes of the Bragg peaks; most prominent are those from the Al can containing the sample.

with AFM propagation vector $\vec{\tau} = (0, 0, \frac{1}{2})$ (in reciprocal-lattice units) consisting of ferromagnetic layers with moments aligned in the ab plane that are stacked antiferromagnetically. The $\chi(T)$ data in the following section confirm that the ordered moments lie in the ab plane.

To confirm the in-plane ferromagnetic (FM) structure we carried out more comprehensive scans to search for additional magnetic peaks. In particular, Fig. 2 shows that no additional magnetic peaks are observed in the difference between scans taken at 4 and 10 K along $(H00)$ [Fig. 2(a)], $(HH0)$ [Fig. 2(b)], $(HH\frac{1}{2})$ [Fig. 2(c)], and $(\frac{1}{2}\frac{1}{2}L)$ [Fig. 2(d)] consistent with a single AFM propagation vector $\vec{\tau} = (0, 0, \frac{1}{2})$. The sharp features in these difference scans are artifacts of the subtraction caused by slight shifts in nuclear Bragg-peak positions due to thermal expansion upon heating. We also performed scans in the (HHL) and (HOL) planes and found additional peaks only at the expected half-integer L positions.

A mean-field analysis of previous single-crystal $\chi(T)$ measurements with $H = 1$ kOe (as opposed to the zero applied magnetic field for the present neutron-diffraction experiments) indicated a c -axis helical magnetic ground state where each adjacent Eu-moment layer is ferromagnetically aligned in the ab plane and rotated by $\approx 120^\circ$ with respect to its nearest-neighbor (NN) Eu layers [8]. If present, such a magnetic structure would give rise to a magnetic unit cell three times that of the chemical unit cell along the c axis, and would be manifested by extra magnetic Bragg reflections shifted from the nuclear Bragg positions by $\pm 1/3$. To search for such reflections or other helical magnetic structures, we conducted scans around prominent magnetic peaks using $E_i = 14.7$ meV. Figure 3 shows a (HOL) two-dimensional map of the intensity at $T = 4$ K minus that taken at 10 K. As shown, we only find

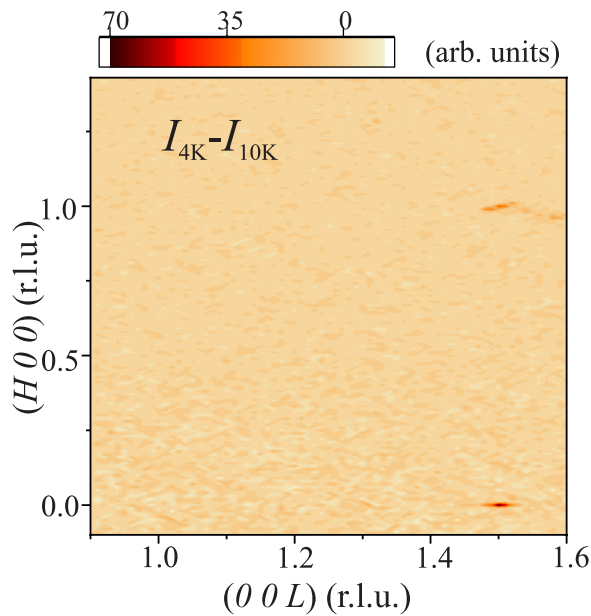


FIG. 3. Two-dimensional $(00L)(H00)$ mesh at $E_i = 14.4$ meV measured at 4 K and after subtracting a similar mesh at 10 K, i.e., in the paramagnetic state above T_N . The reflections $(0\ 0\ 1.5)$ and $(1\ 0\ 1.5)$ are purely magnetic peaks due to a 180° rotation between adjacent layers. The absence of other features in the mesh constitute evidence that there is no 120° helical order at zero applied magnetic field.

peaks at $(0\ 0\ 1.5)$ and at $(1\ 0\ 1.5)$ associated with A-type AFM order and observe no other features; in particular no peaks are found at $L \pm 1/3$ that would correspond to the 120° rotation between NN layers.

The proposed A-type AFM structure is shown in Fig. 4, where adjacent NN FM layers are rotated by 180° with respect to each other. The direction of the FM moment in the Eu layer cannot be determined from neutron diffraction alone. Thus, in Fig. 4 we show two possible magnetic structures where the moments are pointing towards their in-plane NN [Figs. 4(a) and 4(a1)] or to their next-nearest neighbor [Figs. 4(b) and 4(b1)] (there are no additional possibilities according to the Bilbao crystallographic server [14]). Using published values for the structural parameters, we obtain good agreement with the intensities of the nuclear Bragg peaks, both above and below T_N . Based on the above arguments, and assuming equal domain population, we confirm the A-type magnetic structure and obtain an estimate for the ordered magnetic moment $\mu = \langle gS \rangle \mu_B$ at $T = 4$ K using the FULLPROF software [15].

Individual Bragg peaks measured by θ - 2θ scans were fit to Gaussian line shapes to determine their integrated intensities which were then corrected for the geometric Lorentz factor. To account for the significant neutron absorption cross section of Eu, we use the MAG2POL [16] software, by providing the approximate sample shape as a plate of dimensions $2 \times 2 \times 0.5$ mm³. For the refinement of the chemical structure with space group $P\bar{3}m1$ we used published structural parameters [8,9] which we find are in good agreement with our refinement. As noted above, the possible magnetic structures that can occur with a second-order phase transition from space group $P\bar{3}m1$ to AFM order with propagation vector $\vec{\tau} =$

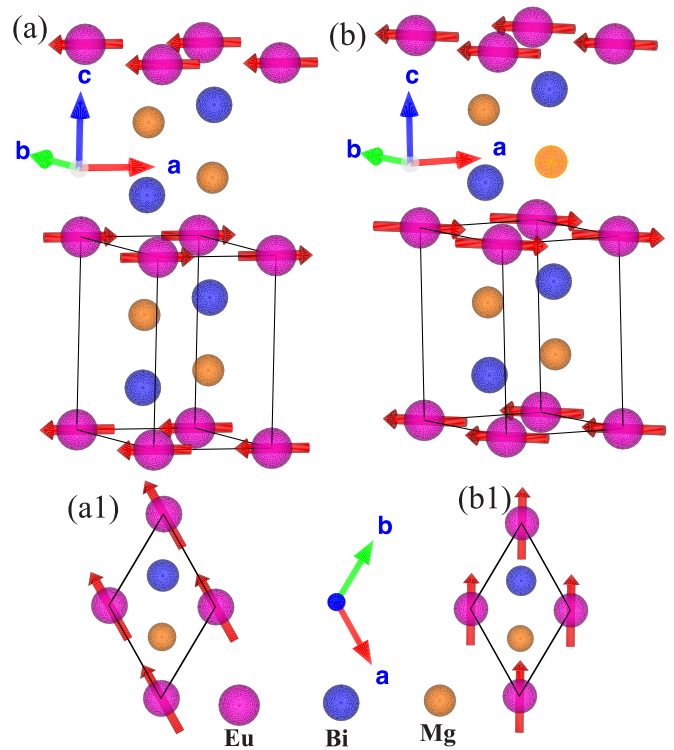


FIG. 4. Chemical and A-type AFM spin structure of EuMg_2Bi_2 . FM spins are aligned towards (a) NN and (b) next-nearest neighbor. (a1) and (b1) show the corresponding projection of a single layer on the ab plane. Our neutron-diffraction data are insensitive to the direction of the FM moment in the plane.

$(0, 0, \frac{1}{2})$ are consistent with antiparallel c axis stacking of FM layers (A-type AFM order). In our analysis of the magnetic structure, we use the C_c2/m (no. 12.63) symmetry [17] [this is the magnetic structure shown in Fig. 4(a) with magnetic moments directed towards NN], and note that our diffraction data eliminate any other minimum symmetry reduction.

Our refinement of the magnetic structure is consistent with the Eu^{2+} form factor and also yields an average magnetic moment $\mu = \langle gS \rangle \mu_B = (5.3 \pm 0.5) \mu_B$ at $T = 4$ K. This value is smaller than the zero-temperature ordered moment $\mu = 7 \mu_B$ expected from the electronic configuration of Eu^{2+} [18] with $S = 7/2$, $L = 0$, and $g = 2$ because μ is not yet saturated to its full value at $T = 0$. Figure 5(a) shows the integrated intensity of the $(0\ 0\ 1/2)$ magnetic peak as a function of temperature where we use a simple power-law function $I_{(0\ 0\ 0.5)}(T) = C|1 - T/T_N|^{2\beta} \propto \mu^2$ to fit the data (solid line with sharp transition). The smooth line around T_N is obtained by the same power law but weighted by a Gaussian distribution of T_N (this form is sometimes used to account for crystal inhomogeneities) yielding $T_N = 6.2 \pm 0.4$ and $\beta = 0.40 \pm 0.05$. The temperature probe in the neutron-diffraction measurements is placed outside the helium-filled aluminum can holding the crystal, likely recording temperatures that are slightly lower than that of the sample. This may explain the discrepancy with the T_N measured by the magnetic susceptibility. Most importantly, the phenomenological fits show that the order parameter is still increasing at $T = 4$ K and not close to its saturated value. Indeed, Fig. 5(b) shows the square root

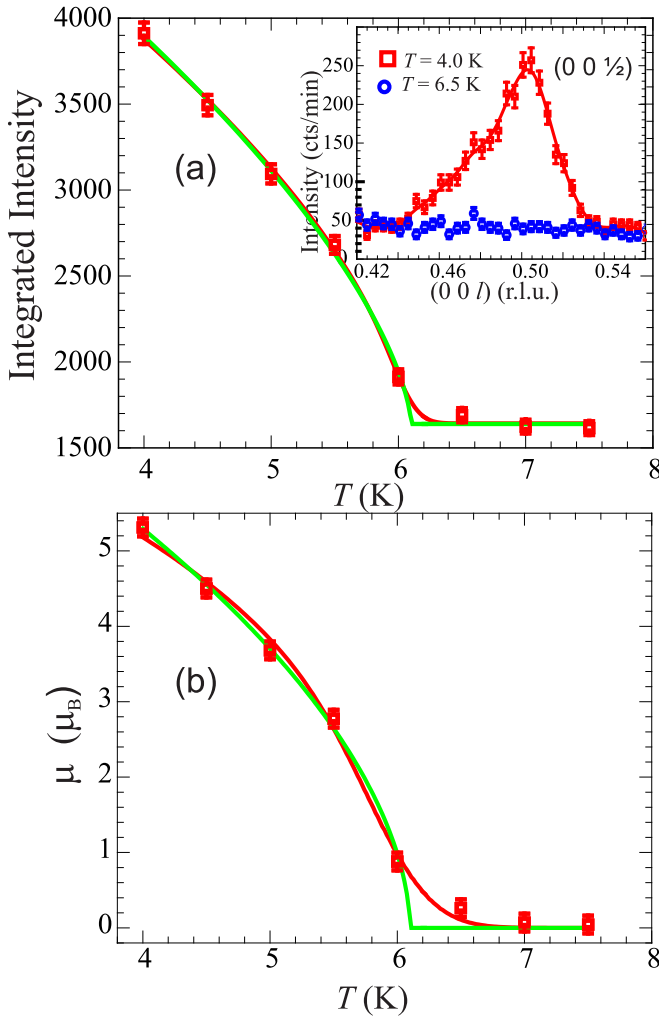


FIG. 5. (a) Integrated intensity as a function of temperature T of the $(0\ 0\ \frac{1}{2})$ magnetic Bragg reflection and (b) calculated ordered moment μ vs T , with a power-law fit (solid green lines) indicating $T_N = (6.2 \pm 0.4)$ K. The red curves in (a) and (b) assume a Gaussian distribution of T_N .

of the data in Fig. 5(a) after subtracting the background and normalizing the value at $T = 4$ K to the extracted average magnetic moment to $\mu(4\text{ K}) = 5.3 \mu_B$. Using the power-law yields $(9.5 \pm 1) \mu_B$ at $T = 0$. This approach overestimates the expected $7 \mu_B$ at $T = 0$ because the phenomenological power-law fit is only accurate just below T_N [13].

IV. MAGNETIC SUSCEPTIBILITY

The difference between the A-type AFM order determined from neutron diffraction at zero field and the reported 120° helical order inferred from bulk susceptibility at 1 kOe [8] suggests that magnetic susceptibility measurements at much lower applied fields should be carried out. Accordingly, we measured the temperature dependence of the magnetic susceptibility $\chi \equiv \frac{M}{H}$ at a very low field $H = 100$ Oe to better approximate the zero-field conditions of our neutron-diffraction data (on a piece of the same single crystal) as shown in Figs. 6(a) and 6(b) for H aligned in the

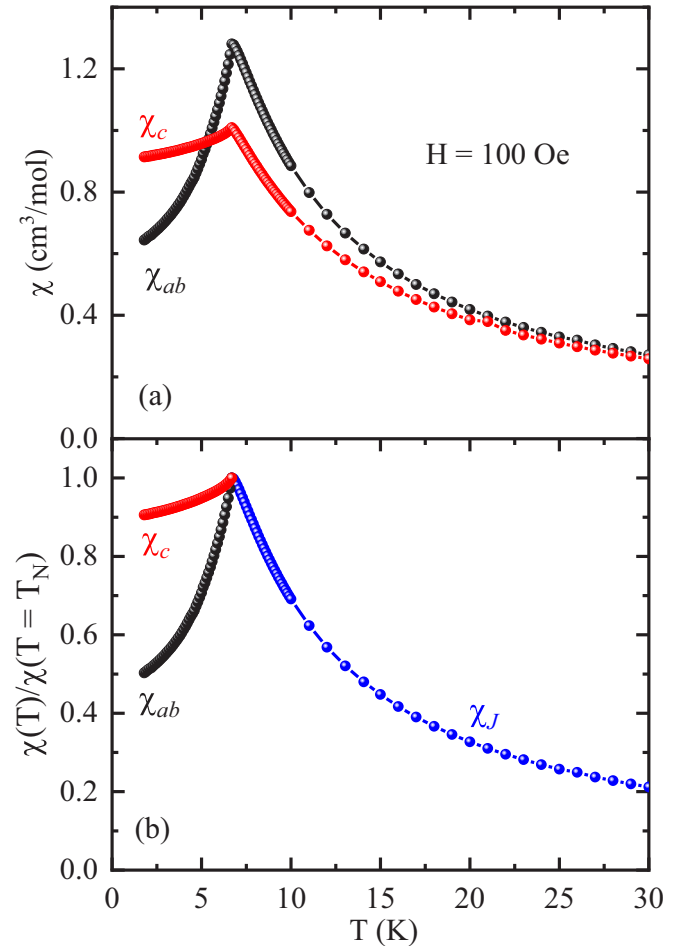


FIG. 6. Temperature dependence of zero-field cooled (ZFC) magnetic susceptibility measured at different applied magnetic fields as listed when the field is (a) in the ab plane ($H \parallel ab$) and (b) along the c axis ($H \parallel c$). In panel (b), the two data sets for $H \parallel ab$ and $H \parallel c$ perfectly overlap in the paramagnetic regime with $T \geq T_N$.

ab plane (χ_{ab}) and along the c axis (χ_c), respectively. The compound orders antiferromagnetically below the Néel temperature $T_N \approx 6.7$ K, as reported earlier [8–10]. Although χ_c in Fig. 6(a) is nearly independent of T below T_N , $\chi_{ab}(H = 100\text{ Oe})$ in Fig. 6(a) decreases by about a factor of 2 upon cooling from T_N to 1.8 K.

To clarify the nature of the ground-state magnetic structure, we analyzed the low-field $\chi(T)$ data in Fig. 6(a) using unified molecular-field theory (MFT) [12,13]. This theory holds for systems of identical crystallographically equivalent spins interacting by Heisenberg exchange and the magnetic properties are calculated from the exchange interactions between an arbitrary spin and its neighbors. According to the MFT, for a c -axis helix χ_c is independent of T below T_N , as seen to be approximately satisfied in Fig. 6(a). However, χ_{ab} is dependent on the turn angle kd for a c -axis helix and is related by

$$\frac{\chi_{Jab}(T=0)}{\chi_J(T_N)} = \frac{1}{2[1 + 2 \cos(kd) + 2 \cos^2(kd)]}, \quad (1)$$

where k is the magnitude of the c -axis helix wave vector in reciprocal-lattice units, d is the distance between the magnetic

layers along the c axis, and the subscript J represents that the anisotropy in $\chi(T \geq T_N)$ has been removed by spherically averaging the anisotropic $\chi(T \geq T_N)$ data; hence the Heisenberg interactions J determine the resulting behavior of the spherically averaged magnetic susceptibility above T_N .

Figure 6(b) depicts the normalized susceptibility $\chi(T)/\chi(T_N)$ of EuMg_2Bi_2 for $H \parallel ab$ and $H \parallel c$, respectively, obtained from the data in Fig. 6(a), yielding $\chi_{ab}(1.8\text{ K})/\chi(T_N) \approx 0.5$. This value is consistent with the A-type structure obtained from neutron diffraction assuming equal populations of three collinear AFM domains oriented at 120° from each other. We note that the A-type AFM implies a turn angle $kd \approx 180^\circ$ in Eq. (1). We also note that good fits to $\chi_{ab}(T)$ data obtained in $H = 1$ kOe for EuCo_2P_2 and $\text{EuNi}_{1.95}\text{As}_2$ crystals with the tetragonal ThCr_2As_2 crystal structure were obtained for c -axis helical structures with turn angles in good agreement with the respective c -axis helical structures previously obtained from zero-field neutron-diffraction measurements [19,20]. However, based on our zero-field diffraction results, the likely scenario is that the higher-field susceptibility data in Ref. [8] are better explained by field-driven spin reorientation rather than by the helical state originally proposed. Only neutron-diffraction measurements in higher applied magnetic fields can confirm this conjecture.

V. CONCLUSION

EuMg_2Bi_2 has drawn interest as it exhibits electronic topological properties that give rise to Dirac-like bands near the Fermi level. The presence of the large-spin Eu^{2+} in the compound makes it attractive since magnetic order can introduce a gap or lower the degeneracy of the Dirac-like bands to create more exotic states, for instance Weyl states. Here, we

use single-crystal zero-field neutron-diffraction and low-field magnetic susceptibility measurements to determine the magnetic ground state of this system.

The neutron-diffraction experiments reveal that the intraplane ordering of $\text{Eu}^{2+}(S = 7/2)$ is ferromagnetic with ab -plane alignment and that adjacent layers are stacked antiferromagnetically (i.e., A-type AFM order). Our detailed analysis also confirms that the ordered magnetic moment, as T approaches 0 K, attains its expected value $\approx 7 \mu_B/\text{Eu}$. The temperature-dependent magnetic susceptibility measurements at a very low magnetic field $H = 100$ Oe applied along the c axis and in the ab plane are consistent with the A-type antiferromagnetism below $T_N = 6.7$ K and also that the moments are aligned in the ab plane. Previous $\chi(T)$ measurements in $H = 1$ kOe indicated that the magnetic structure is a c -axis helix with a 120° turn angle instead of the A-type AFM structure (180° c -axis helix) obtained from our zero-field neutron-diffraction measurements. Neutron-diffraction studies under applied magnetic fields are required to confirm the evolution of the magnetic structure with field inferred from our zero-field neutron-diffraction measurements and the 1-kOe magnetic-susceptibility measurements and are planned for the future.

ACKNOWLEDGMENTS

This research was supported by the U.S. Department of Energy, Office of Basic Energy Sciences, Division of Materials Sciences and Engineering. S.X.M.R. and B.G.U. are supported by the Center for Advancement of Topological Semimetals, an Energy Frontier Research Center funded by the U.S. Department of Energy Office of Science, Office of Basic Energy Sciences, through Ames Laboratory. Ames Laboratory is operated for the U.S. Department of Energy by Iowa State University under Contract No. DE-AC02-07CH11358.

-
- [1] M. Hirschberger, S. Kushwaha, Z. Wang, Q. Gibson, S. Liang, C. A. Belvin, B. A. Bernevig, R. J. Cava, and N. P. Ong, The chiral anomaly and thermopower of Weyl fermions in the half-Heusler GdPtBi , *Nat. Mater.* **15**, 1161 (2016).
- [2] C. Shekhar, N. Kumar, V. Grinenko, S. Singh, R. Sarkar, H. Luetkens, S.-C. Wu, Y. Zhang, A. C. Komarek, E. Kampert, Y. Skourski, J. Wosnitza, W. Schnelle, A. McCollam, U. Zeitler, J. Kübler, B. Yan, H.-H. Klauss, S. S. P. Parkin, and C. Felser, Anomalous Hall effect in Weyl semimetal half-Heusler compounds RPtBi ($R = \text{Gd}$ and Nd), *Proc. Natl. Acad. Sci. USA* **115**, 9140 (2018).
- [3] S. Borisenko, D. Evtushinsky, Q. Gibson, A. Yaresko, K. Koepernik, T. Kim, M. Ali, J. van den Brink, M. Hoesch, A. Fedorov, E. Haubold, Y. Kushnirenko, I. Soldatov, R. Schäfer, and R. J. Cava, Time-reversal symmetry breaking type-II Weyl state in YbMnBi_2 , *Nat. Commun.* **10**, 3424 (2019).
- [4] J.-R. Soh, P. Manuel, N. M. B. Schröter, C. J. Yi, F. Orlandi, Y. G. Shi, D. Prabhakaran, and A. T. Boothroyd, Magnetic and electronic structure of Dirac semimetal candidate EuMnSb_2 , *Phys. Rev. B* **100**, 174406 (2019).
- [5] H. P. Wang, D. S. Wu, Y. G. Shi, and N. L. Wang, Anisotropic transport and optical spectroscopy study on antiferromagnetic triangular lattice EuCd_2As_2 : An interplay between magnetism and charge transport properties, *Phys. Rev. B* **94**, 045112 (2016).
- [6] N. H. Jo, B. Kuthanazhi, Y. Wu, E. Timmons, T. H. Kim, L. Zhou, L. L. Wang, B. G. Ueland, A. Palasyuk, D. H. Ryan, R. J. McQueeney, K. Lee, B. Schruck, A. A. Burkov, R. Prozorov, S. L. Bud'ko, A. Kaminski, and P. C. Canfield, Manipulating magnetism in the topological semimetal EuCd_2As_2 , *Phys. Rev. B* **101**, 140402(R) (2020).
- [7] S. X. M. Riberolles, T. V. Trevisan, B. Kuthanazhi, T. W. Heitmann, F. Ye, D. C. Johnston, S. L. Bud'ko, D. H. Ryan, P. C. Canfield, A. Kreyssig, A. Vishwanath, R. J. McQueeney, L. L. Wang, P. P. Orth, and B. G. Ueland, Magnetic crystalline-symmetry-protected axion electro-dynamics and field-tunable unpinned Dirac cones in EuIn_2As_2 , [arXiv:2007.12758](https://arxiv.org/abs/2007.12758) [Nat. Commun. (to be published)].
- [8] S. Pakhira, M. Tanatar, and D. C. Johnston, Magnetic, thermal, and electronic-transport properties of EuMg_2Bi_2 single crystals, *Phys. Rev. B* **101**, 214407 (2020).
- [9] A. F. May, M. A. McGuire, D. J. Singh, R. Custelcean, and G. E. Jellison, Jr., Structure and properties of single crystalline CaMg_2Bi_2 , EuMg_2Bi_2 , and YbMg_2Bi_2 , *Inorg. Chem.* **50**, 11127 (2011).

- [10] F. Kabir, M. M. Hosen, F. C. Kabeer, A. Aperis, X. Ding, G. Dhakal, K. Dimitri, C. Sims, S. Regmi, L. Persaud, K. Gofryk, P. M. Oppeneer, D. Kaczorowski, and M. Neupane, Observation of multiple Dirac states in a magnetic topological material EuMg_2Bi_2 , [arXiv:1912.08645](#) (2019).
- [11] C. Zheng, R. Hoffmann, R. Nesper, and H. G. von Schnering, Site preferences and bond length differences in CaAl_2Si_2 -type zintl compounds, *J. Am. Chem. Soc.* **108**, 1876 (1986).
- [12] D. C. Johnston, Magnetic susceptibility of collinear and non-collinear Heisenberg antiferromagnets, *Phys. Rev. Lett.* **109**, 077201 (2012).
- [13] D. C. Johnston, Unified molecular field theory for collinear and noncollinear Heisenberg antiferromagnets, *Phys. Rev. B* **91**, 064427 (2015).
- [14] J. M. Perez-Mato, S. V. Gallego, E. S. Tasci, L. Elcoro, G. de la Flor, and M. I. Aroyo, Symmetry-based computational tools for magnetic crystallography, *Annu. Rev. Mater. Res.* **45**, 217 (2015).
- [15] J. Rodríguez-Carvajal, Recent advances in magnetic structure determination by neutron powder diffraction, *Physica B* **192**, 55 (1993).
- [16] N. Qureshi, Mag2Pol: A program for the analysis of spherical neutron polarimetry, flipping ratio and integrated intensity data, *J. Appl. Cryst.* **52**, 175 (2019).
- [17] S. V. Gallego, J. Etxebarria, L. Elcoro, E. S. Tasci, and J. M. Perez-Mato, Automatic calculation of symmetry-adapted tensors in magnetic and non-magnetic materials: A new tool of the Bilbao Crystallographic Server, *Acta Cryst.* **A75**, 438 (2019).
- [18] J. Cable and W. Koehler, Magnetic form factor of Eu^{2+} in EuO , *J. Magn. Magn. Mater.* **5**, 258 (1977).
- [19] N. S. Sangeetha, E. Cuervo-Reyes, A. Pandey, and D. C. Johnston, EuCo_2P_2 : A model molecular-field helical Heisenberg antiferromagnet, *Phys. Rev. B* **94**, 014422 (2016).
- [20] N. S. Sangeetha, V. Smetana, A.-V. Mudring, and D. C. Johnston, Helical antiferromagnetic ordering in $\text{EuNi}_{1.95}\text{As}_2$ single crystals, *Phys. Rev. B* **100**, 094438 (2019).